© 2017. Published by The Company of Biologists Ltd | Journal of Cell Science (2017) 130, 3213-3221 doi:10.1242/jcs.208546

SHORT REPORT

Mosaic loss of non-muscle myosin IIA and IIB is sufficient to induce mammary epithelial proliferation

Kim-Vy Nguyen-Ngoc*, Vanesa L. Silvestri*, Dan Georgess, Amanda N. Fairchild and Andrew J. Ewald‡

ABSTRACT

The mammary epithelium elaborates through hormonally regulated changes in proliferation, migration and differentiation. Non-muscle myosin II (NMII) functions at the interface between contractility, adhesion and signal transduction. It is therefore a plausible regulator of mammary morphogenesis. We tested the genetic requirement for NMIIA and NMIIB in mammary morphogenesis through deletion of the three NMII heavy chain-encoding genes (*NMHCIIA*, *NMHCIIB* and *NMHCIIC*; also known as *MYH9*, *MYH10* and *MYH14*, respectively) that confer specificity to the complex. Surprisingly, mosaic loss, but not ubiquitous loss, of *NMHCIIA* and *NMHCIIB* induced high levels of proliferation in 3D culture. This phenotype was observed even when cells were cultured in basal medium, which does not support tissue level growth of wild-type epithelium. Mosaic loss of NMIIA and NMIIB combined with FGF signaling to induce hyperplasia. Mosaic analysis revealed that the cells that were null for both NMIIA and NMIIB, as well as wild-type cells, proliferated, indicating that the regulation of proliferation is both cell autonomous and non-autonomous within epithelial tissues. This phenotype appears to be mediated by cell–cell contact, as co-culture did not induce proliferation. Mosaic loss of NMIIA and NMIIB also induced excess proliferation *in vivo*. Our data therefore reveal a role for NMIIA and NMIIB as negative regulators of proliferation in the mammary epithelium.

KEY WORDS: Non-muscle myosin IIA, Non-muscle myosin IIB, Mammary epithelial organoid, Cell proliferation, Tissue growth, 3D culture

INTRODUCTION

Cell proliferation and tissue architecture need to be tightly regulated to ensure normal development and homeostasis. Excessive proliferation is a hallmark of cancer and can be induced by constitutive activation of mitogenic signals, inactivation of growth suppressors or escape from contact inhibition of proliferation (Hanahan and Weinberg, 2011). For example, loss of the cadherin–catenin complex can induce uncontrolled proliferation and tumor growth (Jeanes et al., 2008). However, most genetic studies of proliferation have been conducted in conventional 2D cell culture systems, which only partially recapitulate the structure and dynamics of epithelial tissues. The molecular mechanism by which cells sense and regulate proliferation in three-dimensional (3D) tissues remains incompletely understood.

Departments of Cell Biology and Oncology, Center for Cell Dynamics, School of Medicine, Johns Hopkins University, Baltimore, MD 21205, USA.
*These authors contributed equally to this work

‡Author for correspondence (andrew.ewald@jhmi.edu)

A.N.F., 0000-0002-8701-9649; A.J.E., 0000-0002-1964-0740

Received 13 July 2017; Accepted 15 August 2017

Non-muscle myosin II (NMII) is expressed in most cell types and plays an essential role in diverse cellular processes including contractility, adhesion, cytokinesis, migration and signal transduction (Lecuit and Yap, 2015; Ma and Adelstein, 2014). NMII exists in three isoforms: NMIIA, NMIIB, and NMIIC. Each NMII isoform is composed of three pairs of proteins: two regulatory light chains, two essential light chains, and two heavy chains (Vicente-Manzanares et al., 2009). The specificity of the NMII complex is determined by the identity of the heavy chain, which in mammals can be encoded by three genes: NMII heavy chains A, B and C (*NMHCIIA*, *NMHCIIB* and *NMHCIIC*; also known as *MYH9*, *MYH10* and *MYH14*, respectively). NMII molecules bind to and crosslink the actin cytoskeleton to form networks of actomyosin filaments, which support cell architecture and function (Vicente-Manzanares et al., 2009). During single-cell migration, NMII molecules orchestrate integrin-mediated adhesion to extracellular matrix (ECM) substrates (Choi et al., 2008) to ensure directional movement (Yam et al., 2007). In multicellular systems, such as epithelia, NMIIs are required for the establishment and maintenance of apical junctions in early developing tissues, such as the visceral endoderm (Conti et al., 2004) and the spinal neuroepithelium (Ma et al., 2007), and in mature organs, such as the epidermis (Sumigray et al., 2012).

By using a variety of genetic tools, including isoform-specific ablation and replacement, Adelstein and colleagues have discovered both specific and redundant functions for NMII isoforms (Ma and Adelstein, 2014). For example, NMIIA and NMIIB are interchangeable in regulating spinal neuroepithelial intercellular junctions (Ma et al., 2007) whereas NMIIA is uniquely required for mouse placental blood vessel formation, and NMIIB is uniquely required for neuronal cell migration (Ma et al., 2004). Exchanging the two isoforms only partially rescues organ defects in the non-redundant cases. Distinct molecular functions of NMIIA and NMIIB have also been found during the spatio-temporal regulation of E-cadherin-based junctions in epithelial sheets (Smutny et al., 2010). These findings demonstrate the importance of NMII molecules in epithelial tissue architecture and function, and also stimulate questions about how loss of NMII could disrupt tissue homeostasis and promote pathogenesis.

Disruption of NMII-mediated cellular contractility is associated with diverse diseases, including cancer. Cell adhesion to the ECM activates myosin and Rho/ROCK signaling, enabling NMII to mediate both extracellular adhesion and mechanical signals and thereby affect cell behavior (Vicente-Manzanares et al., 2009). Recent studies have also discovered multiple roles for NMII in cancer. For example, sustained elevation of NMII-mediated cellular tension in response to increasing matrix stiffness and rigidity can promote cell proliferation and tumorigenesis (DuFort et al., 2011). NMIIA and NMIIB have distinct roles in force generation and nuclear translocation during cancer invasion (Thomas et al., 2015). Finally, inducible expression of p190-B Rho GTPase (also known

as ARHGAP5) disrupted mammary tissue architecture resulting in increased cell proliferation (Vargo-Gogola et al., 2006). In contrast, reduced contractility due to loss of NMIIA in a tumor-susceptible background promotes cell proliferation and metastasis in squamous cell carcinoma (Schramek et al., 2014). This emerging evidence indicates that NMIIA can be a tumor suppressor; however, the genetic consequences of NMII loss in the normal mammary epithelium remain unclear.

Here, we sought to understand the role of NMII in epithelial organization and development, using the mammary epithelium as a model system. We combined 3D culture of primary epithelial organoids with adenoviral delivery of Cre-recombinase (Ad-Cre) and time-lapse imaging to reveal the cellular consequences of NMII deletion in the mammary epithelium. Surprisingly, we found that mosaic deletion of NMIIA and NMIIB is sufficient to induce epithelial tissue growth and cell proliferation.

RESULTS AND DISCUSSION

Isoform-specific deletion of NMII in mammary organoids

The mammary epithelium consists of two major cell types: an inner luminal epithelial cell layer, surrounded by a basally positioned myoepithelial cell layer. We first examined the expression and localization of NMIIA, NMIIB and NMIIC isoforms within these epithelial populations using both *NMHCIIA–GFP* and *NMHCIIB–GFP* knock-in mice and immunofluorescence staining to detect endogenous proteins (Wang et al., 2010). Consistent with previous reports (Beach et al., 2011), NMIIA was expressed in both luminal and myoepithelial cells, NMIIB was predominantly observed in myoepithelial cells and at low levels near the apical limit of the luminal cell membranes, and NMIIC was restricted to the luminal epithelial cell layer (Fig. S1A–C).

To study the consequences of loss of NMII in the mammary epithelium, we used Cre to delete the *NMHCIIA* and *NMHCIIB* genes in primary mammary organoids, which are fragments of primary epithelial ducts embedded within 3D ECM gels (Matrigel) (Fig. 1A). In these assays, organoids in basal medium (No GF) do not grow without supplemental growth factor addition, but do undergo branching morphogenesis in response to addition of FGF2 or similar growth factors (Ewald et al., 2008; Nguyen-Ngoc et al., 2015). Since the heavy chain confers the specificity of the NMII complex, we refer to the deletion of *NMHCIIA* and *NMHCIIB* and loss of NMIIA and NMIIB interchangeably.

We isolated mammary epithelial organoids from mice carrying both floxed *NMHCIIA* and *NMHCIIB* alleles, and a ubiquitously expressed tamoxifen-inducible Cre (*Cre-ER;NMIIA$^{fl/fl}$;NMIIB$^{fl/fl}$*). Organoids from the same mouse were initially evaluated in three groups: control (untreated), Ad-Cre and tamoxifen (Tam) treatments in basal medium. Infections with Ad-Cre were designed to yield Cre expression in 50–75% of cells (Badea et al., 2003; Shamir et al., 2014). We refer to the organoids treated with Ad-Cre as mosaic NMIIA,B-null organoids. Tamoxifen-induced Cre-ER activity resulted in recombination in essentially all cells. Western blotting confirmed the loss of NMIIA and NMIIB proteins in Tam-treated organoids, and a reduction in both proteins in the Ad-Cre treatment group, while NMIIC protein levels remained unchanged in both treatments (Fig. 1B,C). To analyze the effects of loss of NMIIA and NMIIB in mammary epithelial organoid growth, we measured the fold increase in the projected surface area of the organoids at day 5 compared with that at day 0 in culture.

We observed a significant increase in growth of mosaic organoids compared to that seen in the control and upon Tam treatment, respectively (Fig. 1D; Fig. S2A,C,D). In contrast, control and Tam-treated organoids did not show a significant increase in tissue size. To control for the effects of adenoviral infection, we separately evaluated the consequences of Ad-GFP infection and found no effect on tissue growth (Fig. S2B,G). To control for the effects of Tam on tissue growth, we isolated mammary epithelial organoids from wild-type mice not carrying loxP-flanked *NMHCIIA* and *NMHCIIB* alleles and treated with 50 nM Tam. At the dose used, Tam did not have an effect on organoid growth (Fig. 1D; Fig. S2E–G). These data suggest that NMII is negatively regulating tissue growth.

Mosaic loss of both NMIIA and NMIIB is sufficient to induce hyperproliferation in the mammary epithelium

We investigated the consequences of loss of NMIIA and/or NMIIB in organoids cultured in basal medium (Nguyen-Ngoc et al., 2015). Control epithelial organoids typically maintained their size (Fig. 1E). Deletion of two or three alleles of the *NMHCIIA* and *NMHCIIB* genes did not grossly affect organoid size (Fig. 1F–J). In contrast, mosaic deletion of all four alleles of *NMHCIIA* and *NMHCIIB* genes resulted in tissue growth (Figs 1K and 2A). Strikingly, complete deletion of NMIIA and NMIIB in the Tam-treated organoids did not affect organoid growth, while mosaic deletion with Ad-Cre resulted in a large increase in organoid projected surface area by day 5 in culture (Fig. 1D; Fig. S2C,G, Movie 1). Consistent with this level of tissue growth, mosaic NMIIA,B-null organoids had a higher mitotic index than control organoids, as assayed by staining for phosphorylated histone H3 (pH3) (Fig. 2B–D). Taken together, these data indicate that loss of NMIIA and NMIIB in a mosaic subset of cells is sufficient to induce extensive proliferation in the mammary epithelium, even in basal medium.

Mosaic loss of NMIIA and NMIIB combined with exogenous FGF2 induces hyperplasia

During puberty, mammary epithelial cells undergo branching morphogenesis in response to proliferative signals mediated through steroid hormones and growth factors (Sternlicht et al., 2006). We have previously shown that this process can be modeled through addition of nanomolar concentrations of FGF2 (Ewald et al., 2008; Nguyen-Ngoc et al., 2015). Addition of FGF2 to control organoids induced cell division and resulted in the formation of branched epithelial structures (Fig. S2H), with a corresponding increase in projected surface area relative to initial size (~4-fold, Fig. 2E). Deletion of one to three alleles of the *NMHCIIA* and *NMHCIIB* genes correlated with a non-significant reduction in tissue growth relative to control but was compatible with relatively normal branching (Fig. S2I–M). In contrast, mosaic deletion of all four alleles in FGF2-treated organoids led to a significant increase in tissue growth over time (~9-fold), as inferred from the change in projected surface area of organoids in time-lapse movies (Fig. 2E; Fig. S2N). Consistent with the tissue growth in time-lapse movies, mosaic NMIIA,B-null organoids had a higher mitotic index than control organoids, as assayed by pH3 staining (Fig. 2F–H). These data demonstrate that loss of both NMIIA and NMIIB can combine with FGF2 signaling to further promote excess proliferation. Taken together, we conclude that NMIIA and NMIIB together serve as negative regulators of proliferation within the mammary epithelium.

Mosaic loss of NMIIA and NMIIB induces both cell autonomous and non-autonomous proliferation within the mammary epithelium

We next asked whether the excess proliferation was limited to NMIIA, B-null cells. To address this question, we introduced a convertible double-fluorescent Cre reporter into the floxed myosin II line,

Journal of Cell Science (2017) 130, 3213-3221 doi:10.1242/jcs.208546

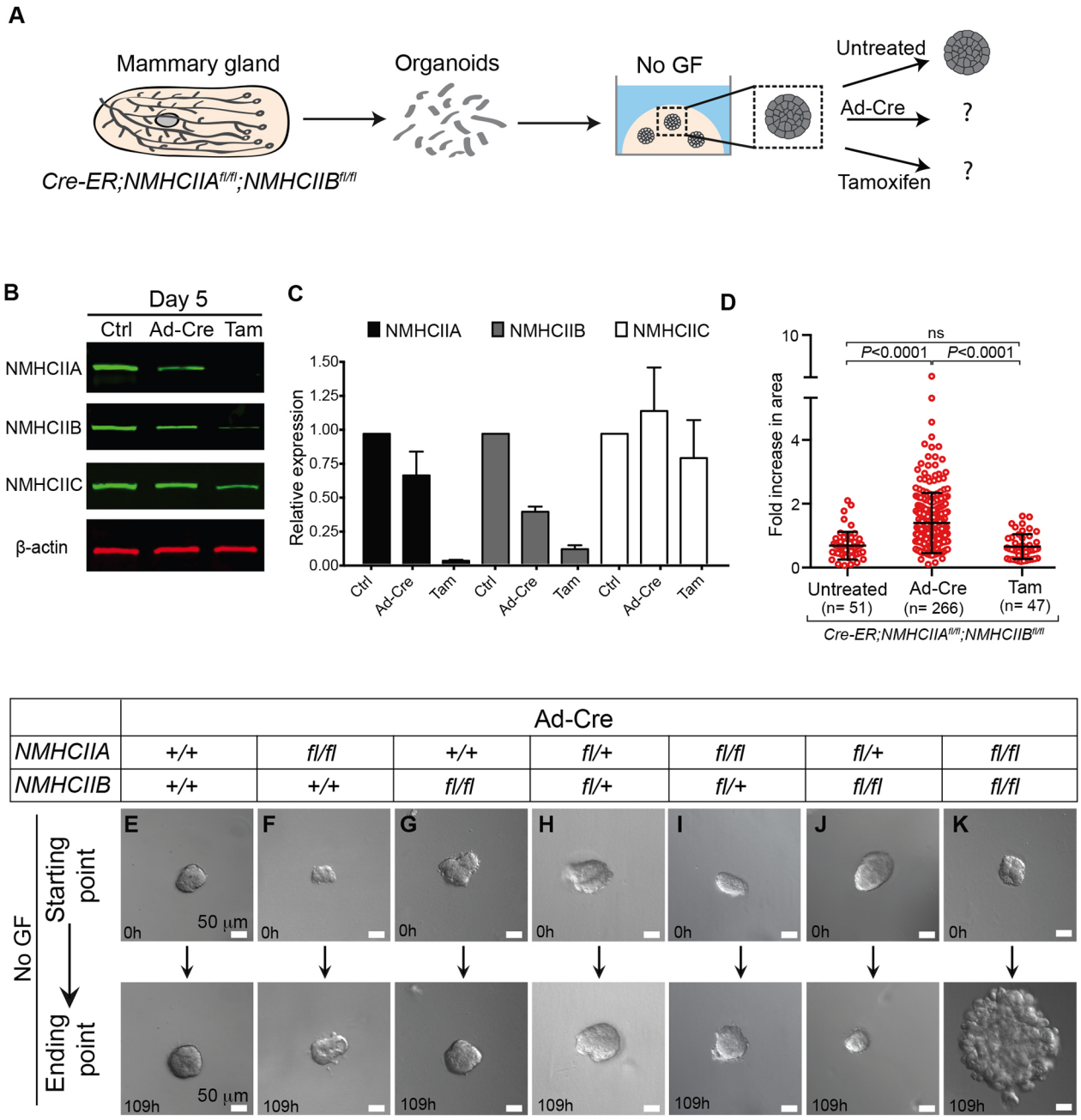

Fig. 1. Concurrent loss of both NMIIA and NMIIB in a subset of cells in the mammary epithelium is sufficient to induce tissue growth. (A) Schematic representation of 3D organotypic culture of *Cre-ER;NMIIA*$^{fl/fl}$*;NMIIB*$^{fl/fl}$ mammary epithelial organoids in basal medium (No GF). Organoids from the same mouse are divided into three groups for control (untreated), adenoviral Cre recombinase (Ad-Cre) or tamoxifen (Tam) treatments. Ad-Cre was used to accomplish mosaic recombination and tamoxifen induced the Cre-ER to recombine ubiquitously. (B) Representative western blot and (C) protein quantification showing a reduction of NMIIA and NMIIB proteins levels in organoids after Ad-Cre and Tam treatments, respectively (n=3 mice; whole-organoid lysate samples were loaded for equal protein based on BCA analysis). (D) Mammary organoid growth was evaluated by determining the fold increase in projected surface area of organoids at day 5 compared to that at day 0 in culture. Data are presented as mean±s.d. n, number of organoids summed across three biologically independent experiments. P<0.0001; ns, non-significant as indicated (one-way ANOVA). (E–K) Still images from time-lapse movies of organoids carrying different combinations of NMIIA and NMIIB floxed alleles, treated with Ade-Cre in basal medium without growth factor (Movie 1). Scale bars: 50 µm.

NMIIA$^{fl/fl}$*;NMIIB*$^{fl/fl}$*;mTmG*. In this model, all cells constitutively express membrane-localized tdTomato (red fluorescence) and, upon Ad-Cre treatment, switch heritably to expression of membrane-localized GFP. Therefore, green fluorescence serves as a direct reporter for Cre activity and an indirect reporter for *NMHCIIA* and *NMHCIIB* gene deletion. *NMIIA*$^{fl/fl}$*;NMIIB*$^{fl/fl}$*;mTmG* organoids were treated with Ad-Cre to generate a mixture of red and green cells. Mosaic organoids were then embedded in 3D Matrigel in basal medium. This strategy allowed us to identify which population of cells, wild-type (red, Cre−) or NMIIA,B-null (green, Cre+), contributed to the overgrowth phenotype (Fig. 3A).

Since we observed a significant increase in proliferation in Ad-Cre-treated organoids by 70–80 h in culture (Fig. 2A), we collected fluorescent confocal *z*-stack images at day 3 and day 5 (Fig. 3B,D). To calculate the contributions of wild-type and NMIIA,B-null cells, we measured the total volume of each population of cells for each

Journal of Cell Science (2017) 130, 3213-3221 doi:10.1242/jcs.208546

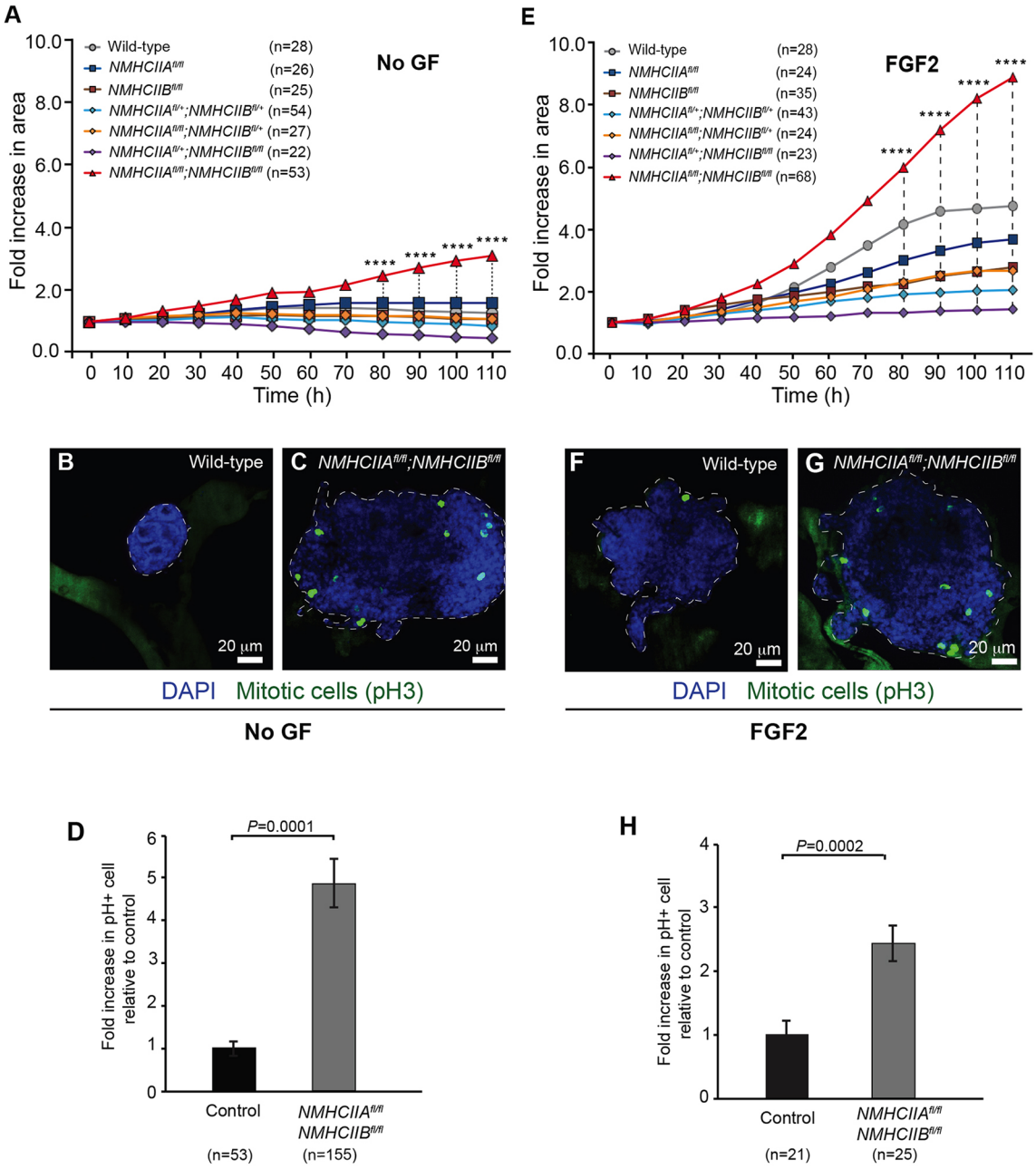

Fig. 2. Mosaic loss of NMIIA and NMIIB induces proliferation in mammary organoids cultured in basal medium or with FGF2 supplementation. (A) The growth rate of organoids carrying different numbers of floxed alleles of NMIIA and NMIIB treated with Ad-Cre in basal medium (No GF) was determined by measuring the projected surface area of the organoid normalized to initial size. (B,C) Confocal images of mammary organoids in basal medium stained to label proliferation (pH3, green) and nuclei (blue). (D) The fold increase in the number of pH3+ cells in organoids in basal medium was calculated by dividing the number of pH3+ cells by the number of cells per organoid presented relative to that in control (set at 1). (E) The growth rate of organoids carrying different numbers of floxed alleles of NMIIA and NMIIB treated with Ad-Cre in FGF2-supplemented medium was determined by measuring the projected area of the organoid normalized to initial size. (F,G) Confocal images of organoids in FGF2-supplemented medium stained to label proliferation (pH3, green) and nuclei (blue). (H) The fold increase in pH3+ cells of organoids in FGF2-supplemented medium was calculated by dividing the number of pH3+ cells by the organoid projected surface area presented relative to that in control (set at 1). n, number of organoids summed across three biologically independent experiments. *P<0.0001 (A,E) for difference in growth rate across samples within the same time point (one-way ANOVA). In D,H, results are mean±s.e.m. and P-values were calculated with a Mann–Whitney test. White dashed lines in B,C,F,G mark the shape of organoids.

mosaic organoid at day 3 (initial volume) and day 5 (final volume) of culture by performing 3D surface rendering (Fig. 3C,E). Using initial and final surface-rendered volumes of wild-type and NMIIA, B-null cells (Fig. 3F,G), we calculated and compared growth rates. We found that the percentage change in volume for NMIIA,B-null cells was 101.5% compared to 41% for wild-type cells (Fig. 3H). Time-lapse movies also confirmed that the increase in volume was due to increased cell proliferation and not cell growth (Movie 2; Fig. S3A–C). We validated successful completion of cytokinesis by evaluating cell shapes in 3D in confocal time-lapse movies and speculate that it could be accomplished due to residual NMIIC (Fig. 1B). We conclude that loss of NMIIA and NMIIB induce both cell autonomous and non-autonomous proliferation in mammary epithelium.

Journal of Cell Science (2017) 130, 3213-3221 doi:10.1242/jcs.208546

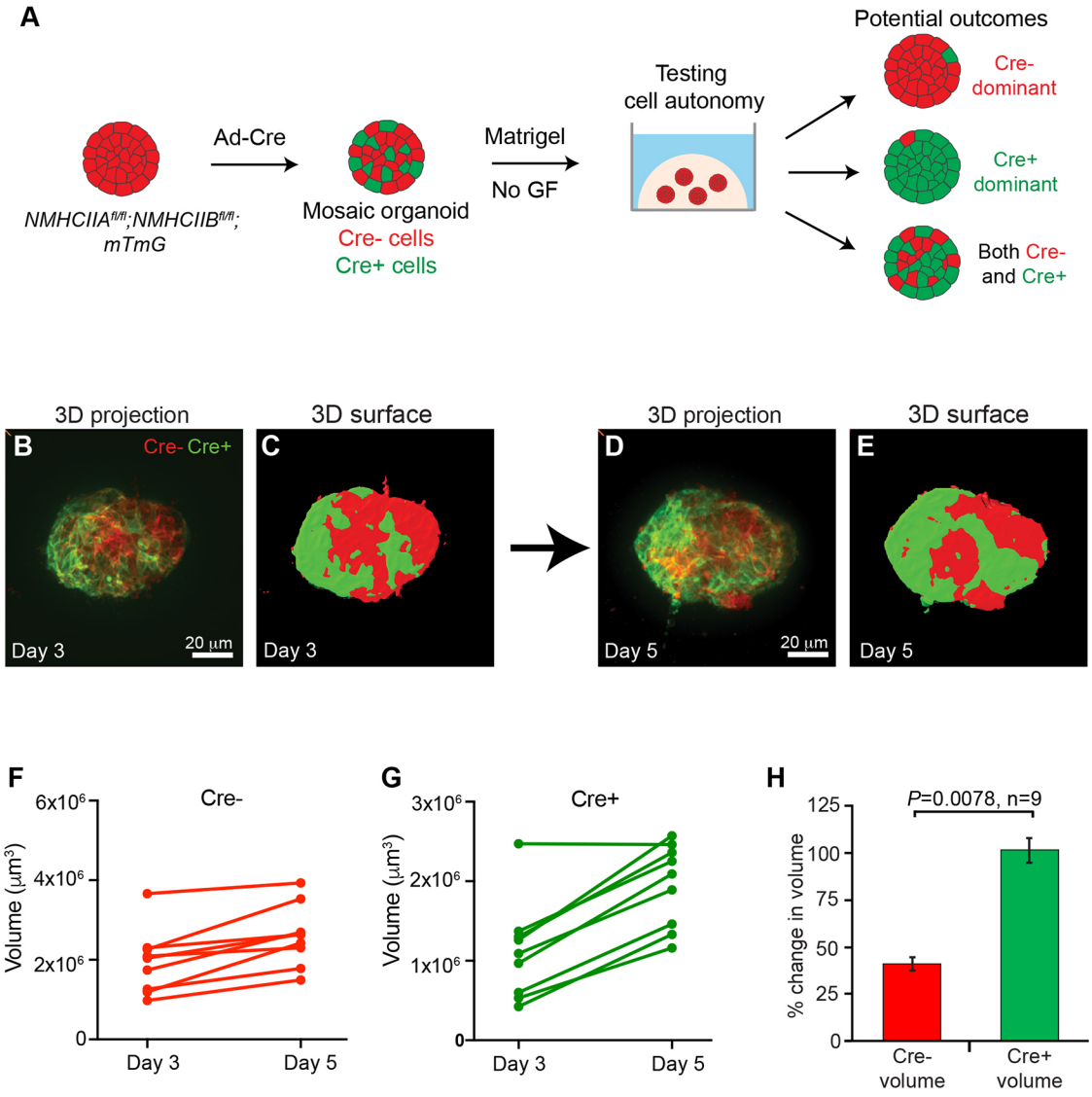

Fig. 3. Heterogeneous loss of NMIIA and NMIIB induces proliferation of cells null for both NMIIA and NMIIB, and wild-type cells within the mammary epithelium. (A) Organoids isolated from *Cre-ER;NMIIA$^{fl/fl}$;NMIIB$^{fl/fl}$;mTmG* mice were treated with Ad-Cre to generate a mixture of Cre– (red) and Cre+ (green) cells. Mosaic organoids were plated in 3D Matrigel in basal medium (No GF) to test cell autonomy. There were three potential outcomes: (1) Cre+ dominant, (2) Cre– dominant or (3) a mixture of both Cre+ and Cre– cells. (B,D) Representative 3D projection and (C,E) 3D surface rendering of a mosaic organoid at day 3 and day 5 in culture. (F–G) Plots of initial and final surface-rendered volumes of red and green cells, respectively. (H) Percentage change in volume of Cre– and Cre+ cells. Results are mean±s.e.m. *P*-values were determined by the Mann–Whitney test. n, number of organoids summed across three biologically independent experiments.

Hyperproliferation induced by mosaic loss of NMIIA and NMIIB is not mediated by soluble factors

Having demonstrated that wild-type and NMIIA,B-null cells proliferate in response to mosaic loss of NMIIA and IIB within an organoid, we next sought to determine whether this effect was mediated by soluble factors. To test this hypothesis, we used the *NMIIA$^{fl/fl}$;NMIIB$^{fl/fl}$;mTmG* line to generate both wild-type (containing only red cells) and Ad-Cre-treated organoids (mixture of red and green cells) for mosaic NMIIA,B deletion as described above. We then co-cultured wild-type and mosaic organoids in a 1:1 ratio in 3D Matrigel with basal medium (Fig. 4A). Confocal microscopy images were taken at day 5 in culture (Fig. 4B–D). To analyze differences in growth, we measured the projected area of organoids in co-culture compared to that of wild-type (control) and mosaic (control) organoids, respectively. We observed a consistent and significant 2.5-fold increase in growth of mosaic organoids in both monoculture and co-culture, relative to wild-type (Fig. 4E). In contrast, wild-type organoids essentially did not increase in size in either monoculture or co-culture (Fig. 4E). Taken together, these data suggest that the hyperproliferation caused by mosaic deletion of NMIIA and NMIIB in mammary organoids is not mediated by soluble factors but is instead likely mediated by cell–cell contact.

Deletion of both NMIIA and NMIIB increases sporadic cell proliferation in epithelial ducts *in vivo*

Our genetic analysis in 3D culture revealed that mosaic loss of NMIIA and NMIIB resulted in excess proliferation in both wild-type and NMIIA,B-null cells. We next tested the consequences of NMIIA and NMIIB deletion in polarized mammary epithelium *in vivo*. We isolated and orthotopically transplanted organoids from *Cre-ER;NMIIA$^{fl/fl}$;NMIIB$^{fl/fl}$;mTmG* and *CreER;NMIIA$^{fl/+}$;mTmG* (control) mice into the cleared mammary fat pad of non-fluorescent

Journal of Cell Science (2017) 130, 3213-3221 doi:10.1242/jcs.208546

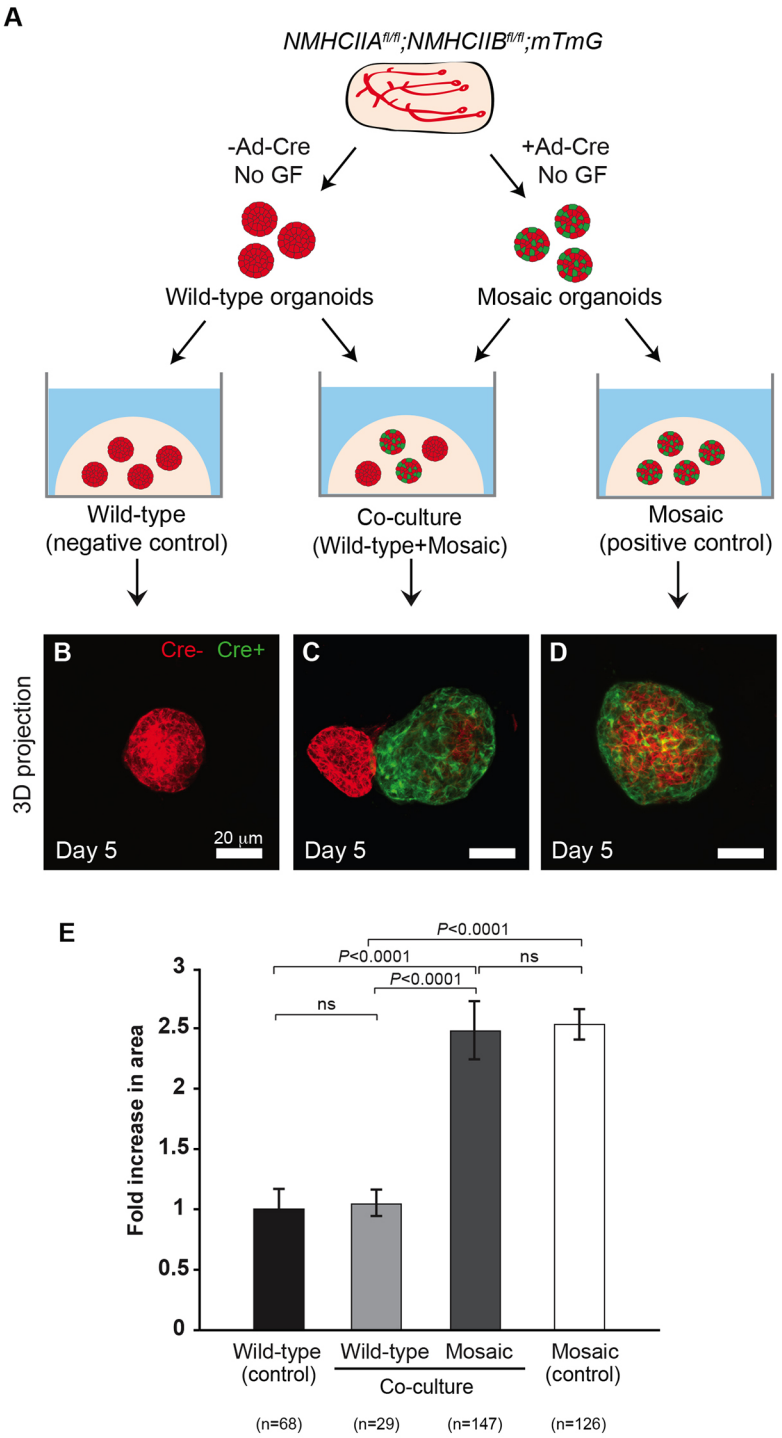

Fig. 4. Coculture of mosaic NMIIA- and NMIIB-null organoids with wild-type organoids reveal that the hyperproliferation is restricted to the mosaic epithelium. (A) Control and genetic mosaic organoids from the same mouse were mono-cultured or co-cultured in a 1:1 ratio (control organoid:mosaic organoid) in basal medium (No GF) for 5 days. Representative 3D projection images for (B) wild-type (negative control) (C) co-culture (wild-type plus mosaic organoids) and (D) mosaic organoids (positive control) at day 5 in culture. (E) Fold increase in mammary organoid growth was calculated by measuring projected surface area compared to that of the wild-type control (set at 1). Results are mean±s.e.m. ****P<0.0001; ns, non-significant (Mann–Whitney test). n, number of organoids summed across three biologically independent experiments. Scale bars: 20 µm.

host mice. We allowed 6 weeks for ductal network formation, then induced NMIIA and NMIIB deletion by tamoxifen injection and waited an additional 6 weeks before collecting mammary glands (Fig. S4A) to assay proliferation by pH3 staining. Similar to the organoids cultured in basal medium without additional growth factors, control epithelium contained very few pH3+ mitotic cells (Fig. S4B,C). In contrast, epithelia where NMIIA and NMIIB were deleted displayed an increased number of mitotic cells (Fig. S4B′,C′). We calculated the number of proliferative cells per field of view (40× objective) and observed a statistically significant increase following loss of NMIIA and NMIIB (Fig. S4D). Finally, proliferation was observed in both red (Cre−) and green (Cre+) cells demonstrating that the effect of NMIIA,B deletion on proliferation was also both cell autonomous and non-autonomous *in vivo* (Fig. S4E′–G). The magnitude of the increase in proliferation and the associated disruption of epithelial architecture were both smaller *in vivo* compared to that seen *in vitro*. We speculate that this difference is due to the presence of additional negative regulators of proliferation, to differences in the extent of mosaicism in the epithelium or to differential protein stability.

Our genetic analysis of NMII was motivated by previous pharmacological studies in which inhibition of myosin activity disrupted branching morphogenesis in multiple organs (Daley et al., 2009; Ewald et al., 2008; Meyer et al., 2006; Michael et al., 2005;

Moore et al., 2005). Our data support the concept that NMII can function as a negative regulator of proliferation. NMII-mediated tension regulates the establishment and dynamics of intercellular junctions (Smutny et al., 2010), and loss of junctional components such as E-cadherin (Derksen et al., 2006) accelerates mammary tumor progression. Cell tension derived from NMII-based contractility is required to support these adhesion complexes and also responds to the forces generated by adjacent cells and the ECM (Lecuit and Yap, 2015). Therefore, either an elevation or reduction of myosin activity could change cell behavior and tissue organization. We therefore speculate that mosaic but not ubiquitous loss of NMII isoforms could induce proliferation by destabilizing intercellular junctions or disrupting mechanotransduction.

NMIIA and NMIIB are essential for multiple functions at the cell and tissue level, and so deletion of all four alleles may be statistically unlikely in cancer cells. However, a similar heterogeneity in myosin activity across the tissue could be achieved through clonal loss of myosin inhibitors or clonal gain of activators. These mechanisms would phenocopy the effect of NMIIA and NMIIB deletion in a subset of cells and could drive clonal fixation in either the myosin-deficient or neighboring myosin-normal cells. As an example, overexpression of p190-B Rho GTPase induces hyperplasia in the mammary epithelium (Vargo-Gogola et al., 2006). Given the ubiquity of disruptions in Rho GTPase signaling in human cancer (Sahai and Marshall, 2002; Vega and Ridley, 2008), we speculate that heterogeneity in myosin levels between neighboring cells could be a major driver of cancer cell proliferation.

MATERIALS AND METHODS

Mouse strains

The NMIIA$^{fl/fl}$, NMIIB$^{fl/fl}$, NMIIA–GFP and NMIIB–GFP knock-in mouse lines (Jacobelli et al., 2010; Ma et al., 2009) were a gift from Robert Adelstein (National Heart, Lung, and Blood Institute, NIH, Bethesda, MD). The *R26::Cre-ER* mouse line was a gift of Jeremy Nathans (Johns Hopkins University, Baltimore, MD). The *FVB/NJ*, *mT/mG* (Muzumdar et al., 2007) and NOD.Cg-*Prkdcscid Il2rgtm1Wjl/SzJ* (NSG) mouse lines were acquired from the Jackson Laboratory. Mouse husbandry and procedures were all conducted according to an animal protocol approved by the Johns Hopkins University School of Medicine Institutional Animal Care and Use Committee.

3D culture assays of primary mammary epithelial organoids

We used a combined mechanical and enzymatic digestion with collagenase (C2139; Sigma-Aldrich) and trypsin (27250-018; Gibco Life Technologies), followed by differential centrifugation to isolate groups of mammary epithelial ducts, termed organoids, from 10- to 12-week-old mice as previously described (Ewald et al., 2008; Nguyen-Ngoc et al., 2015). Organoids were then embedded in 3D growth factor-reduced Matrigel™ (354230; Corning) at 2–3 organoids/µl as 150 µl suspensions in a 24-well multiwell glass-bottom plate (662892; Greiner Bio-One) or in two-well chamber coverglass (155379; ThermoFisher Scientific). Gels were allowed to polymerize for 30 min at 37°C and then cultured in minimal medium [DMEM/F12 (10565-018, Gibco), 1% v/v insulin, transferrin, selenium (51500, ThermoFisher) and 1% (v/v) penicillin-streptomycin (15140-122, Gibco)]. Basal medium conditions (No GF) refer to organoids embedded in growth factor-reduced Matrigel and cultured in minimal medium without the addition of supplemental growth factors. For the branching morphogenesis assay, minimal medium is supplemented with 2.5 nM FGF2 (F0291, Sigma).

Tamoxifen-inducible Cre-mediated deletion in 3D culture

Cre activity was induced in *Cre-ER;NMIIA$^{fl/fl}$;NMIIB$^{fl/fl}$;mT/mG* mammary epithelium by culturing organoids embedded in 3D Matrigel with 50 nM tamoxifen (T5648; Sigma-Aldrich) for 18 h. Cultures were then rinsed with PBS to wash out tamoxifen and incubated in fresh organoid medium for 5 days at 37°C. The tamoxifen-inducible system resulted in Cre activity in essentially all cells but did not have obvious morphological consequences for wild-type organoids.

Adenoviral gene delivery

As previously described (Huebner et al., 2016; Shamir et al., 2014), prior to embedding in 3D Matrigel, organoids were infected with Adenoviral-GFP or Adenoviral-CMV-Cre (Vector BioLabs) at ∼10^7 plaque-forming units (PFU) per 1000 organoids. Infections were conducted in 50 µl DMEM for 1.5 h at 37°C. Following viral treatment, organoids were washed twice in DMEM/F12 and suspended in Matrigel as described above.

Orthotopic transplantation to mammary fat pad

For transplantation of mammary organoids followed by induction of gene deletion, we isolated and incubated organoids overnight at 37°C in organoid medium with 2.5 nM FGF2 in HydroCell 96-well microplates (174907, Thermo Fisher Scientific). The next day, organoids were suspended in a 50% DMEM:50% Matrigel solution at a density of 20–30 organoids/µl and kept on ice throughout the procedure. We conducted orthotopic transplantations into the cleared mammary fat pads of 3- to 4-week-old NSG mice in a sterile hood. In brief, mice were anesthetized with 2–2.5% isoflurane and immobilized, and the surgical site was cleaned with ethanol. The mammary gland was exposed by a 1 cm mid-sagittal cut followed by a 0.5 cm oblique cut from the initial incision to one hip. The skin was then retracted to expose the number 4 mammary gland. The number 5 gland and the lymph node in the number 4 gland were removed. Then, 10–20 µl of organoid suspension was injected into the number 4 gland using a syringe (702RN[7636–01]; Hamilton; custom 1 inch needles, 26 gauge). The skin was then locally infiltrated with 5–10 µl of 0.25% bupivacaine. The same procedure was repeated in the contralateral mammary gland. For each mouse, we transplanted control organoids (*Cre-ER;NMIIA$^{fl/+}$;mTmG*) in one gland and experimental organoids (*Cre-ER;NMIIA$^{fl/fl}$;NMIIB$^{fl/fl}$;mTmG*) in the other. The wounds were closed with 9-mm autoclips. Triple antibiotic ointment was applied to wounding sites. Deletion of NMIIA and NMIIB in mature ductal networks was accomplished at 6 weeks post transplantation by injection of 100 µl of 10 mg/ml tamoxifen by intraperitoneal injection every other day for 5 days (three total injections) using a 1 ml syringe and a 30G1/2 needle (305106; BD Biosciences). Glands were harvested 6 weeks after tamoxifen injection.

Differential interference contrast microscopy

Time-lapse imaging was performed with an LD Plan-Neofluar 20×/0.4 Korr Ph2 objective lens and a Cell Observer system with an AxioObserver Z1 and an AxioCam MRM camera (Carl Zeiss). In general, 100–200 positions were captured in parallel at 20 min intervals for 5 days. Temperature was set at 37°C and CO_2 at 5%. AxioVision (Carl Zeiss) software was used to acquire and analyze the movies, place scale bars and export time frames as TIFF images. Photoshop CS6 (Adobe) was used to adjust levels and brightness across entire images to maximize image clarity.

Confocal microscopy

Confocal imaging was conducted on a spinning-disk confocal microscope (Solamere Technology Group, Inc.) with an XR/MEGA-10 S30 camera (Stanford Photonics, Inc.) as previously described (Ewald, 2013). A Fluar 20×/0.75 objective lens (Carl Zeiss) was used for intermediate magnification images, an LD C-Apochromat 40×/1.1 W Korr objective lens (Carl Zeiss) was used for high-magnification single and time-lapse image acquisition, with water and Immersol™ W 2010 (Zeiss) used as the imaging mediums, respectively. Acquisition was performed with a combination of µManager (Edelstein et al., 2010) and Piper (Stanford Photonics, Inc.) software. For time-lapse imaging to observe cell division, images were captured at 20-min intervals for 16–18 h, and the temperature was set at 37°C and CO_2 at 5%. Imaris (Bitplane) was used to analyze images, add scale bars and export individual TIFF images. Photoshop CS6 (Adobe) was used to adjust levels and to perform gamma correction for each channel, across the entire image, to maximize image clarity.

Immunofluorescence staining

Organoids and mammary gland tissues were collected, fixed and stained as previously described (Nguyen-Ngoc et al., 2015). Briefly, organoids embedded in 3D Matrigel and whole mammary glands were fixed in 4% paraformaldehyde for 15 min and 3 h, respectively. The samples were then

rinsed three time with PBS for 10 min, embedded in Optimal Cutting Temperature (OCT) compound, and stored at −80°C. OCT blocks were sectioned at 100 µm thickness for cultured organoid samples and 50 µm thickness for gland tissue. Sections were placed on Superfrost Plus Gold microscope slides (15-188-48; Fisherbrand) and stored at −80°C. For antibody staining, slides were thawed at room temperature, rinsed twice with PBS to remove OCT and permeabilized with 0.5% Triton X-100 for 1 h. Samples were then blocked with 10% fetal bovine serum (FBS) and 1% bovine serum albumin (BSA) in PBS for 2–3 h and incubated with primary antibody solution overnight at 4°C in 1% FBS and 1% BSA in PBS. Slides were then rinsed twice in PBS with 10% FBS and 1% BSA and then incubated with secondary antibodies diluted in PBS with 1% FBS and 1% BSA overnight at 4°C. Slides were rinsed twice in PBS with 1% FBS and 1% BSA for 10 min and once in PBS for 10 min, mounted with Fluoromount (F4680; Sigma-Aldrich), and sealed with coverslips. Nuclei were stained with DAPI (1:1000, D3571, Invitrogen). Immunofluorescent staining for each antibody was done for at least three independent biological replicates. Mouse anti-phospho-H3 (1:300, 9706L, Cell Signaling Technology) was used as primary antibody and Alexa Fluor 647-conjugated goat anti-mouse-IgG (1:200, Invitrogen) as secondary antibody.

Protein extraction

Lysis buffer was prepared by diluting 10× RIPA buffer (20-188; EMD Millipore) with ultrapure water and incubating on ice for 2 h. Immediately before addition to cell pellets, lysis buffer was supplemented with 0.1% SDS, 5% glycerol, 3 mM EDTA, 1 mM NaF, 1 mM PMSF, 1.5 mM $NaVO_4$, aprotinin (A6279; Sigma-Aldrich) and a mini protease inhibitor tablet (11836153001; Roche). Organoids embedded in 3D Matrigel were collected for protein extraction as follows: the medium was aspirated, the gels were rinsed once with 1 ml cold PBS, and then dissolved in 1 ml cold PBS/EDTA buffer (5 mM EDTA, 1 mM $NaVO_4$, 1.5 mM NaF and 1 mM PMSF in PBS). The suspensions were then transferred to centrifuge tubes, mixed well by pipetting, incubated on a shaker for 1 h at 4°C, and centrifuged at 211 ***g*** for 5 min at 4°C. Supernatants were removed and pellets were suspended with 50–100 µl of RIPA lysis buffer. The suspension was left on ice for 40–60 min and vortexed every 10 min. Tubes were centrifuged for 10 min at 15,700 ***g*** at 4°C. Supernatants were transferred to fresh tubes and stored at −80°C.

Western blotting

Cell lysates were thawed or directly used after preparation. Samples were mixed with Laemmli sample buffer (161-0747; Bio-Rad Laboratories), β-mercaptoethanol and heated at 70°C for 10 min. Samples were loaded for equal amounts of protein based on bicinchoninic acid (BCA) analysis (Thermo Fisher Scientific) in 4–15% Mini-PROTEAN TGX precast gels (456-1084; Bio-Rad Laboratories). SDS-PAGE was performed at 115 V for 1 h. Gels were transferred onto Immobilon-FL membranes (IPFL07810; Millipore) at 100 V for 1 h at 4°C. Membranes were blocked in 10 ml Odyssey Blocking Buffer for 1 h at room temperature on a shaker before incubation with primary antibody in 50:50 Odyssey Blocking Buffer/TBST (Tris-buffered saline with 0.1% Tween-20) at 4°C overnight. Primary antibodies used were rabbit anti-NMIIA (1:1000; 909801; BioLegend), rabbit anti-NMIIB (1:1000; 909901; BioLegend), rabbit anti-NMIIC (1:1000; 919201; BioLegend) and mouse anti-β-tubulin (1:1000; T5201; Sigma) antibodies. Membranes were washed three times with TBST for 5 min, before incubation with secondary antibodies (IR-conjugated Licor) in 50:50 Odyssey blocking buffer/TBST for 1 h at room temperature on a shaker. Secondary antibodies used were goat anti-rabbit-IgG conjugated to 800CW (1:10,000, 827-08365; Licor) and goat anti-mouse-IgG conjugated to 680RD (1:10,000; 926-68170; Licor). Membranes were then washed twice with TBST for 5 min and once with TBS for 5 min, before being imaged wet on the Licor Odyssey CLx imaging system. Bands were quantified using ImageJ.

Quantification and statistical analysis

Image analyses were performed using ImageJ and Imaris software (Bitplane Scientific, Zurich, Switzerland). All statistical analyses were conducted using STATA or Graphpad Prism. Data was evaluated for normality using a D'Agostino–Pearson omnibus test. The *P*-value was determined by one-way ANOVA or a Mann–Whitney test if the data did not present a normal distribution. $P<0.05$ was considered significant. Column plots report mean± s.e.m. All data represent at least three biological replicates.

Acknowledgements

We thank members of the Ewald laboratory for helpful discussions. We thank Seyvonne Ip for help with image acquisition and Alex Choi for help with image analysis. We thank Mary Anne Conti and Robert Adelstein for provision of mice and technical advice.

Competing interests

The authors declare no competing or financial interests.

Author contributions

Conceptualization: K.-V.N.-N., V.L.S., A.J.E.; Methodology: K.-V.N.-N., V.L.S., D.G., A.N.F., A.J.E.; Validation: D.G., A.N.F., K.-V.N.-N, V.L.S. and A.J.E.; Formal analysis: K.-V.N.-N., V.L.S., D.G., A.J.E.; Investigation: K.-V.N.-N., V.L.S., D.G., A.N.F.; Writing - original draft: K.-V.N.-N., V.L.S., A.J.E.; Writing - review & editing: K.-V.N.-N., V.L.S., D.G., A.N.F., A.J.E.; Visualization: K.-V.N.-N., V.L.S.; Supervision: A.J.E.; Project administration: A.J.E.; Funding acquisition: A.J.E.

Funding

D.G. is funded by a postdoctoral fellowship grant from the Susan G. Komen for the Cure foundation (PDF15332336). A.J.E. received support for this project from the Commonwealth Foundation, the Breast Cancer Research Foundation/Pink Agenda (BCRF-16-048), a grant from the National Institutes of Health (National Cancer Institute) (U54 CA2101732), the Isaac and Lucille Hay Fellowship, and the Climb for Hope foundation. Deposited in PMC for release after 12 months.

Supplementary information

Supplementary information available online at
http://jcs.biologists.org/lookup/doi/10.1242/jcs.208546.supplemental

References

Badea, T. C., Wang, Y. and Nathans, J. (2003). A noninvasive genetic/pharmacologic strategy for visualizing cell morphology and clonal relationships in the mouse. *J. Neurosci.* **23**, 2314-2322.

Beach, J. R., Hussey, G. S., Miller, T. E., Chaudhury, A., Patel, P., Monslow, J., Zheng, Q., Keri, R. A., Reizes, O., Bresnick, A. R. et al. (2011). Myosin II isoform switching mediates invasiveness after TGF-beta-induced epithelial-mesenchymal transition. *Proc. Natl. Acad. Sci. USA* **108**, 17991-17996.

Choi, C. K., Vicente-Manzanares, M., Zareno, J., Whitmore, L. A., Mogilner, A. and Horwitz, A. R. (2008). Actin and alpha-actinin orchestrate the assembly and maturation of nascent adhesions in a myosin II motor-independent manner. *Nat. Cell Biol.* **10**, 1039-1050.

Conti, M. A., Even-Ram, S., Liu, C., Yamada, K. M. and Adelstein, R. S. (2004). Defects in cell adhesion and the visceral endoderm following ablation of nonmuscle myosin heavy chain II-A in mice. *J. Biol. Chem.* **279**, 41263-41266.

Daley, W. P., Gulfo, K. M., Sequeira, S. J. and Larsen, M. (2009). Identification of a mechanochemical checkpoint and negative feedback loop regulating branching morphogenesis. *Dev. Biol.* **336**, 169-182.

Derksen, P. W. B., Liu, X., Saridin, F., van der Gulden, H., Zevenhoven, J., Evers, B., van Beijnum, J. R., Griffioen, A. W., Vink, J., Krimpenfort, P. et al. (2006). Somatic inactivation of E-cadherin and p53 in mice leads to metastatic lobular mammary carcinoma through induction of anoikis resistance and angiogenesis. *Cancer Cell.* **10**, 437-449.

DuFort, C. C., Paszek, M. J. and Weaver, V. M. (2011). Balancing forces: architectural control of mechanotransduction. *Nat. Rev. Mol. Cell Biol.* **12**, 308-319.

Edelstein, A., Amodaj, N., Hoover, K., Vale, R. and Stuurman, N. (2010). Computer control of microscopes using microManager. *Curr. Protoc. Mol. Biol.* Chapter 14, Unit 14.20.

Ewald, A. J. (2013). Practical considerations for long-term time-lapse imaging of epithelial morphogenesis in three-dimensional organotypic cultures. *Cold Spring Harb. Protoc.* **2013**, 100-117.

Ewald, A. J., Brenot, A., Duong, M., Chan, B. S. and Werb, Z. (2008). Collective epithelial migration and cell rearrangements drive mammary branching morphogenesis. *Dev. Cell* **14**, 570-581.

Hanahan, D. and Weinberg, R. A. (2011). Hallmarks of cancer: the next generation. *Cell* **144**, 646-674.

Huebner, R. J., Neumann, N. M. and Ewald, A. J. (2016). Mammary epithelial tubes elongate through MAPK-dependent coordination of cell migration. *Development* **143**, 983-993.

Jacobelli, J., Friedman, R. S., Conti, M. A., Lennon-Dumenil, A.-M., Piel, M., Sorensen, C. M., Adelstein, R. S. and Krummel, M. F. (2010).

Confinement-optimized three-dimensional T cell amoeboid motility is modulated via myosin IIA-regulated adhesions. *Nat. Immunol.* **11**, 953-961.
Jeanes, A., Gottardi, C. J. and Yap, A. S. (2008). Cadherins and cancer: how does cadherin dysfunction promote tumor progression? *Oncogene* **27**, 6920-6929.
Lecuit, T. and Yap, A. S. (2015). E-cadherin junctions as active mechanical integrators in tissue dynamics. *Nat. Cell Biol.* **17**, 533-539.
Ma, X. and Adelstein, R. S. (2014). The role of vertebrate nonmuscle Myosin II in development and human disease. *Bioarchitecture* **4**, 88-102.
Ma, X., Kawamoto, S., Hara, Y. and Adelstein, R. S. (2004). A point mutation in the motor domain of nonmuscle myosin II-B impairs migration of distinct groups of neurons. *Mol. Biol. Cell* **15**, 2568-2579.
Ma, X., Bao, J. and Adelstein, R. S. (2007). Loss of cell adhesion causes hydrocephalus in nonmuscle myosin II-B-ablated and mutated mice. *Mol. Biol. Cell* **18**, 2305-2312.
Ma, X., Takeda, K., Singh, A., Yu, Z.-X., Zerfas, P., Blount, A., Liu, C., Towbin, J. A., Schneider, M. D., Adelstein, R. S. et al. (2009). Conditional ablation of nonmuscle myosin II-B delineates heart defects in adult mice. *Circ. Res.* **105**, 1102-1109.
Meyer, T. N., Schwesinger, C., Sampogna, R. V., Vaughn, D. A., Stuart, R. O., Steer, D. L., Bush, K. T. and Nigam, S. K. (2006). Rho kinase acts at separate steps in ureteric bud and metanephric mesenchyme morphogenesis during kidney development. *Differentiation* **74**, 638-647.
Michael, L., Sweeney, D. E. and Davies, J. A. (2005). A role for microfilament-based contraction in branching morphogenesis of the ureteric bud. *Kidney Int.* **68**, 2010-2018.
Moore, K. A., Polte, T., Huang, S., Shi, B., Alsberg, E., Sunday, M. E. and Ingber, D. E. (2005). Control of basement membrane remodeling and epithelial branching morphogenesis in embryonic lung by Rho and cytoskeletal tension. *Dev. Dyn.* **232**, 268-281.
Muzumdar, M. D., Tasic, B., Miyamichi, K., Li, L. and Luo, L. (2007). A global double-fluorescent Cre reporter mouse. *Genesis (New York, N.Y. : 2000)* **45**, 593-605.
Nguyen-Ngoc, K.-V., Shamir, E. R., Huebner, R. J., Beck, J. N., Cheung, K. J. and Ewald, A. J. (2015). 3D culture assays of murine mammary branching morphogenesis and epithelial invasion. *Methods Mol. Biol.* **1189**, 135-162.
Sahai, E. and Marshall, C. J. (2002). RHO-GTPases and cancer. *Nat. Rev. Cancer* **2**, 133-142.
Schramek, D., Sendoel, A., Segal, J. P., Beronja, S., Heller, E., Oristian, D., Reva, B. and Fuchs, E. (2014). Direct in vivo RNAi screen unveils myosin IIa as a tumor suppressor of squamous cell carcinomas. *Science (New York, N.Y.)* **343**, 309-313.
Shamir, E. R., Pappalardo, E., Jorgens, D. M., Coutinho, K., Tsai, W.-T., Aziz, K., Auer, M., Tran, P. T., Bader, J. S. and Ewald, A. J. (2014). Twist1-induced dissemination preserves epithelial identity and requires E-cadherin. *J. Cell Biol.* **204**, 839-856.
Smutny, M., Cox, H. L., Leerberg, J. M., Kovacs, E. M., Conti, M. A., Ferguson, C., Hamilton, N. A., Parton, R. G., Adelstein, R. S. and Yap, A. S. (2010). Myosin II isoforms identify distinct functional modules that support integrity of the epithelial zonula adherens. *Nat. Cell Biol.* **12**, 696-702.
Sternlicht, M. D., Kouros-Mehr, H., Lu, P. and Werb, Z. (2006). Hormonal and local control of mammary branching morphogenesis. *Differentiation* **74**, 365-381.
Sumigray, K. D., Foote, H. P. and Lechler, T. (2012). Noncentrosomal microtubules and type II myosins potentiate epidermal cell adhesion and barrier formation. *J. Cell Biol.* **199**, 513-525.
Thomas, D. G., Yenepalli, A., Denais, C. M., Rape, A., Beach, J. R., Wang, Y.-L., Schiemann, W. P., Baskaran, H., Lammerding, J. and Egelhoff, T. T. (2015). Non-muscle myosin IIB is critical for nuclear translocation during 3D invasion. *J. Cell Biol.* **210**, 583-594.
Vargo-Gogola, T., Heckman, B. M., Gunther, E. J., Chodosh, L. A. and Rosen, J. M. (2006). P190-B Rho GTPase-activating protein overexpression disrupts ductal morphogenesis and induces hyperplastic lesions in the developing mammary gland. *Mol. Endocrinol* **20**, 1391-1405.
Vega, F. M. and Ridley, A. J. (2008). Rho GTPases in cancer cell biology. *FEBS Lett.* **582**, 2093-2101.
Vicente-Manzanares, M., Ma, X., Adelstein, R. S. and Horwitz, A. R. (2009). Non-muscle myosin II takes centre stage in cell adhesion and migration. *Nat. Rev. Mol. Cell Biol.* **10**, 778-790.
Wang, A., Ma, X., Conti, M. A., Liu, C., Kawamoto, S. and Adelstein, R. S. (2010). Nonmuscle myosin II isoform and domain specificity during early mouse development. *Proc. Natl Acad. Sci. USA* **107**, 14645-14650.
Yam, P. T., Wilson, C. A., Ji, L., Hebert, B., Barnhart, E. L., Dye, N. A., Wiseman, P. W., Danuser, G. and Theriot, J. A. (2007). Actin-myosin network reorganization breaks symmetry at the cell rear to spontaneously initiate polarized cell motility. *J. Cell Biol.* **178**, 1207-1221.